Available online at www.sciencedirect.com
ScienceDirect
Journal of the European Ceramic Society 27 (2007) 3135–3140
www.elsevier.com/locate/jeurceramsoc

Static fatigue behavior of cracked piezoelectric ceramics in three-point bending under electric fields

Yasuhide Shindo *, Fumio Narita, Fumitoshi Saito

Department of Materials Processing, Graduate School of Engineering, Tohoku University, Aoba-yama 6-6-02, Sendai 980-8579, Japan

Received 14 September 2006; received in revised form 16 November 2006; accepted 25 November 2006
Available online 6 February 2007

Abstract

This paper describes an experimental and analytical study on the static fatigue behavior of piezoelectric ceramics under electromechanical loading. Static fatigue tests were carried out in three-point bending with the single-edge precracked-beam specimens. The crack was created perpendicular to the poling direction. Time-to-failure under different mechanical loads and dc electric fields were obtained from the experiment. Microscopic examination of the fracture surface of the piezoelectric ceramics was performed as well. A finite element analysis was also made, and the applied energy release rate for the permeable crack model was calculated. The effect of applied dc electric fields on the energy release rate versus lifetime curve is examined. The most important conclusion we reach is that the lifetimes for the piezoelectric specimens under a positive electric field are much shorter than the failure times of specimens under a negative electric field for the same mechanical load level.

Keywords: PZT; Mechanical properties; Fatigue

1. Introduction

Lead zirconate titanate (PZT) ceramics are widely used in piezoelectric devices, e.g., sensors and actuators. The high mechanical stresses and intense electric fields in the PZT ceramics may cause microcracks to develop which eventually lead to failure of the devices. The fracture behavior of the PZT ceramics under electromechanical loading has been the subject of recent studies. In the calculations of piezoelectric fracture mechanics parameters such as energy release rate, there are two commonly used electrical boundary conditions across the crack face, (1) the permeable crack model and (2) the impermeable crack model. Park and Sun[1] performed mode I and mixed mode fracture tests on the PZT ceramics using three-point bending, and discussed the fracture behavior based on the mechanical strain energy release rate of the impermeable crack. Fu and Zhang[2] conducted compact tension and indentation fracture tests to study the effect of applied electric fields on the fracture toughness. They ignored electroelastic interactions of piezoelectric materials, and obtained the apparent fracture toughness. Shindo et al.[3] made single-edge precracked beam tests and corresponding finite element analysis to calculate the energy release rate using the permeable and impermeable cracks, and found that the permeable crack model is valid for the analysis of piezoelectric crack problems. Soh et al.[4] also found that strain energy density criterion for the impermeable crack is unable to describe the effect of electric fields on piezoelectric fracture behavior. Furthermore, test data and analysis of Jelitto et al.[5] did not comply with the fracture criteria based on the total or mechanical energy release rate of the impermeable crack. As seen in the previous works, the trend of the fracture mechanics parameters for the permeable crack is consistent with the experimental results. On the other hand, Shindo et al.[6] investigated theoretically and experimentally the fracture and polarization properties of the PZT ceramics under mechanical and electrical loads ultilizing the modified small punch test technique. They found that polarization switching in a local region has a significant influence on the piezoelectric fracture behavior. Shindo et al.[7] also performed double torsion tests and corresponding nonlinear finite element analysis. The results showed that polarization switching near a crack tip leads to an unexpected nonlinearity in the piezoelectric fracture mechanics parameters.

To begin addressing the influence of electric fields on fatigue of piezoelectric materials, fatigue crack propagation has been

* Corresponding author. Tel.: +81 22 795 7341; fax: +81 22 795 7341.
E-mail address: shindo@material.tohoku.ac.jp (Y. Shindo).

0955-2219/$ – see front matter © 2006 Elsevier Ltd. All rights reserved.
doi:10.1016/j.jeurceramsoc.2006.11.078

demonstrated in the PZT ceramics with a surface crack produced by Vickers indentation under cyclic electric loading.[8,9] Recently, Lee et al.[10] conducted experiments on the PZT ceramics with a through-thickness crack, and discussed the cyclic electric-field-induced fatigue. Fang et al.[11] also investigated cyclic electric-field-induced fatigue in PZT ceramics with a short notch. They showed that under low electric fields, the emergence and growth of microcracks is the major fatigue mechanism that impedes the growth of the main crack, whereas the main crack is the only mode of fatigue cracking under high electric fields. On the other hand, Salz et al.[12] studied crack growth under cyclic mechanical load in PZT ceramics. A V-shaped notch was oriented parallel to the poling direction, and the specimens were loaded in four-point bending without an electric field.

It is known that electric fields can affect the fatigue life of the piezoelectric devices under sustained mechanical loading. In recent years, the effect of electric fields on the delayed fracture of PZT ceramics in silicon oil[13] was investigated. However, electroelastic interactions were ignored, and only the stress intensity factor for (elastic) metals was used in their discussions. Literature studies of fatigue in the PZT ceramics under both mechanical and electrical loads are sparse and inconclusive.

In this study, we present experimental and numerical results on the fatigue behavior of piezoelectric ceramics under constant applied mechanical and electric fields using three-point bending methods. The time-to-failure was measured as a function of constant applied load and dc electric field, based on experiments using single-edge precracked-beam specimens. A static fatigue effect characterized by a energy release rate dependence was also observed, in combination with the finite element method. The data suggest that the lifetime of the piezoelectric ceramics depends very strongly on the applied electric field. Possible mechanisms of static fatigue in piezoelectric ceramics under electromechanical loading are discussed.

2. Experimental procedure

The experimental geometry is shown in Fig. 1. The essential experimental parameters are crack length, a; span, S; and applied load, P_0. The size of the specimens was nominally 5 mm thick, 5 mm wide, and 15 mm long. Poling was done along the axis of the 15 mm dimension.

Specimens were commercially supplied hard PZT ceramics PCM-80 (Matsushita Electric Industrial Co., Ltd., Japan). The material properties are listed in Table 1 and the average grain size is 1–3 μm. Through-thickness crack was produced using the method previously described.[3] This method basically involves the extension of a small starter crack produced by Vickers indentation into a diminishing stress field created by the application of a bridge anvil into the surface of a piezoelectric specimen (see Fig. 2(a)). The crack so produced was about 0.5 mm. Fig. 2(b) shows a photograph of the precrack.

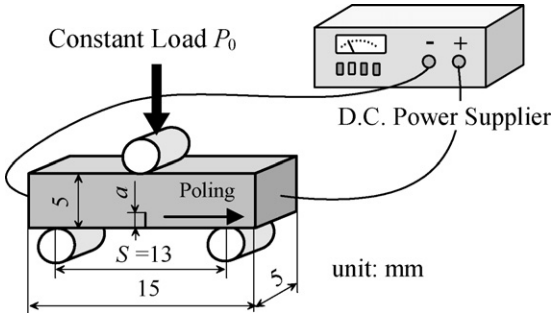

Fig. 1. Specimen configuration.

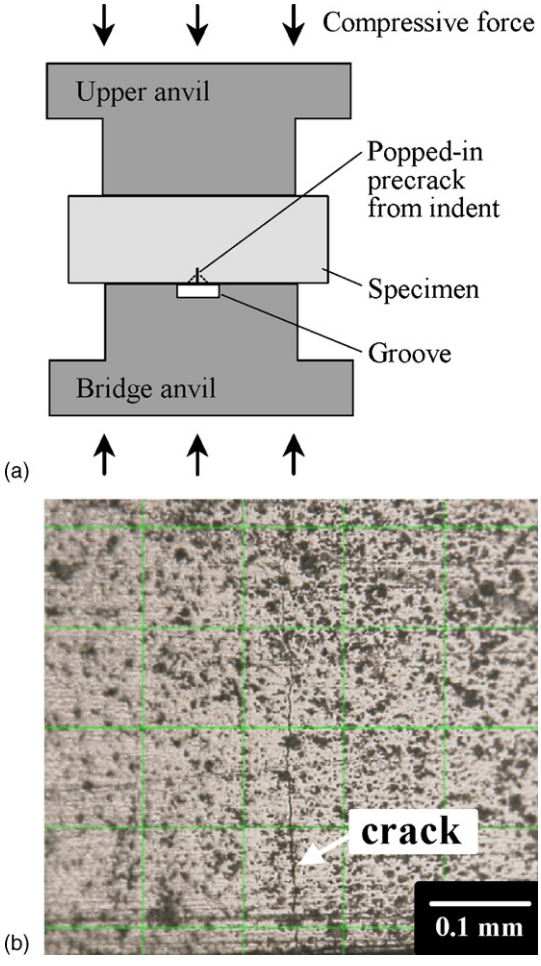

Fig. 2. (a) Schematic of a bridge anvil mechanism for forming precracks in piezoelectric specimens. (b) Photograph showing a piezoelectric crack.

Table 1
Material properties of PCM-80

	Elastic stiffnesses ($\times 10^{10}$ N/m^2)					Piezoelectric coefficients (C/m^2)			Dielectric constants ($\times 10^{-10}$ C/V m)	
	c_{11}	c_{33}	c_{44}	c_{12}	c_{13}	e_{31}	e_{33}	e_{15}	$\in_{11}$	$\in_{33}$
PCM-80	17.0	16.5	3.05	10.6	11.5	−5.99	15.6	13.7	95.2	68.4

Three-point bending apparatus with a span of $S = 13$ mm were used for the static fatigue tests. A 250 N load cell (resolution: 0.01 N) was employed to apply the load to the specimen. Time-to-failure under a constant applied load at three different load levels was measured. Crack motion was observed through a ×1000microscope, and the appropriate energy release rates required for a given load were calculated using finite element method. All tests were conducted at room temperature. After testing, a scanning electron microscope (SEM) was used to examine static fatigue and overload fracture surfaces. Due to cost and time constraints, the number of specimens was limited.

3. Analysis

3.1. Basic equations

Consider a linear piezoelectric material with no body force and free charge. The governing equations in the Cartesian coordinates x_i ($i = 1, 2, 3$) are given by

$$\sigma_{ji,j} = 0 \tag{1}$$

$$D_{i,i} = 0 \tag{2}$$

where σ_{ij} is the stress tensor, D_i the electric displacement vector, u_i the displacement vector, a comma denotes partial differentiation with respect to the coordinate x_i, and the Einstein summation convention over repeated indices is used. The relation between the strain tensor ε_{ij} and the displacement vector u_i is given by

$$\varepsilon_{ij} = \frac{1}{2}(u_{j,i} + u_{i,j}) \tag{3}$$

and the electric field intensity is

$$E_i = -\phi_{,i} \tag{4}$$

where ϕ is the electric potential. Constitutive relations can be written as

$$\sigma_{ij} = c_{ijkl}\varepsilon_{kl} - e_{kij}E_k \tag{5}$$

$$D_i = e_{ikl}\varepsilon_{kl} + \in_{ik} E_k \tag{6}$$

where c_{ijkl} and e_{ikl} are the elastic and piezoelectric constants, $\in_{ik}$ is the dielectric permittivity, and

$$\begin{aligned} &c_{ijkl} = c_{jikl} = c_{ijlk} = c_{klij}, \qquad e_{kij} = e_{kji} \\ &\in_{ik} = \in_{ki} \end{aligned} \tag{7}$$

The constitutive Eqs. (5) and (6) for PZT poled in the x_3-direction are found in Appendix A.

3.2. Finite element model

Plane strain finite element calculations were made to determine the energy release rate for the cracked piezoelectric specimens. The specimen and loading geometries are shown in Fig. 3. A rectangular Cartesian coordinate system (x, y, z) is used with the z-axis coinciding with the poling direction.

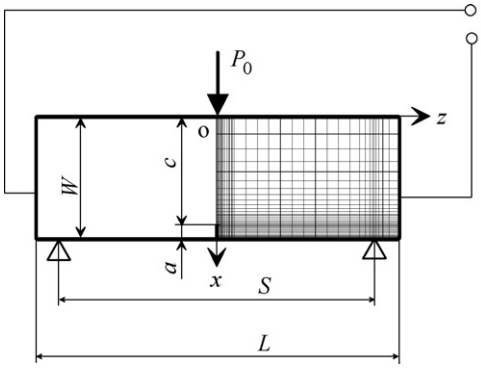

Fig. 3. Schematic diagram of the finite element model.

A mechanical load was produced by the application of a prescribed force P_0 at $x = 0, z = 0$ along the x-direction. For electrical loads, a negative or positive electric potential ϕ_0 was applied at the edge $0 \le x \le W, z = L/2$. The edge $0 \le x \le W$, $z = -L/2$ was grounded. The electric potential applied at the edge $0 \le x \le W$, $z = L/2$ produced an electric field $E_0 = -\phi_0/L$. A positive (negative) electric field was produced by the application of a negative (positive) electric potential at the edge $0 \le x \le W, z = L/2$. Due to symmetry, only the right half of the model was used in the finite element analysis. Four-node plane elements in ANSYS were used. The total number of nodes and elements are 930 and 870, respectively.

The mechanical and electrical boundary conditions can be written as

$$\sigma_{zx}(x, 0) = 0 \quad (0 \le x \le W) \tag{8}$$

$$\begin{cases} u_z(x, 0) = 0 & (0 \le x \le c) \\ \sigma_{zz}(x, 0) = 0 & (c < x \le W) \end{cases} \tag{9}$$

$$\begin{cases} \phi(x, 0) = 0 & (0 \le x \le c) \\ E_x(x, 0) = E_x^c(x, 0) & (c < x \le W) \\ D_z(x, 0) = D_z^c(x, 0) & (c < x \le W) \end{cases} \tag{10}$$

$$\sigma_{zz}\left(x, \frac{L}{2}\right) = 0 \quad (0 \le x \le W) \tag{11}$$

$$\sigma_{zx}\left(x, \frac{L}{2}\right) = 0 \quad (0 \le x \le W) \tag{12}$$

$$\phi\left(x, \frac{L}{2}\right) = \frac{\phi_0}{2} \quad (0 \le x \le W) \tag{13}$$

$$\sigma_{xx}(0, z) = -P_0\delta(z) \tag{14}$$

$$\sigma_{xx}(0, z) = 0 \quad \left(0 < z \le \frac{L}{2}\right) \tag{15}$$

$$\sigma_{xz}(0, z) = 0 \quad \left(0 \le z \le \frac{L}{2}\right) \tag{16}$$

$$D_x(0, z) = 0 \quad \left(0 \le z \le \frac{L}{2}\right) \tag{17}$$

$$\sigma_{xx}(W, z) = 0 \quad \left(0 \le z < \frac{S}{2}, \frac{S}{2} < z \le \frac{L}{2}\right) \tag{18}$$

$$u_x\left(W, \frac{S}{2}\right) = 0 \tag{19}$$

$$\sigma_{xz}(W, z) = 0 \quad \left(0 \le z \le \frac{L}{2}\right) \tag{20}$$

$$D_x(W, z) = 0 \quad \left(0 \le z \le \frac{L}{2}\right) \tag{21}$$

where the superscript c stands for the electric quantity in the void inside the crack and $\delta(z)$ is the Dirac-delta function. Eq. (10) are the permeable crack boundary conditions. The electric potential is all zero on the symmetry planes inside the crack and ahead of the crack, so the boundary conditions of Eq. (10) reduce to $\phi(x, 0) = 0\,(0 \le x \le W)$. The electric field intensity $E_x^c(x, 0)$ is equal to zero, and the electric displacement $D_z^c(x, 0)$ is determined precisely. The condition of Eq. (13) gives the electric field $E_0 = -\phi_0/L$.

The energy release rate G can be obtained from the following crack-tip integral:

$$G = \int_{\Gamma_0} \{Hn_x - (\sigma_{xx}u_{x,x} + \sigma_{zx}u_{z,x})n_x - (\sigma_{zx}u_{x,x} + \sigma_{zz}u_{z,x})n_z + D_xE_xn_x + D_zE_xn_z\}\,\mathrm{d}\Gamma \tag{22}$$

where Γ_0 is a small contour closing a crack tip and n_x, n_z are the components of the outer unit normal vector. The electrical enthalpy density H is expressed as

$$H = \frac{1}{2}\{c_{11}(u_{x,x})^2 + c_{33}(u_{z,z})^2 + 2c_{13}u_{x,x}u_{z,z} + c_{44}(u_{x,z} + u_{z,x})^2\} - \frac{1}{2}\{\in_{11}(E_x)^2 + \in_{33}(E_z)^2\} - \{e_{15}(u_{x,z} + u_{z,x})E_x + (e_{31}u_{x,x} + e_{33}u_{z,z})E_z\} \tag{23}$$

4. Results and discussion

The experimental data on the static fatigue of hard PZT ceramics PCM-80 under applied electric field $E_0 = +0.1, 0$, and -0.1 MV/m are summarized in Fig. 4. The fracture test results (averages of three measurements for each electric field) on PCM-80 are also shown. Some specimens failed before reaching 130 N of applied load (see Table 2). Times-to-failure t_f of the PZT ceramics under static loading in general exhibited behavior

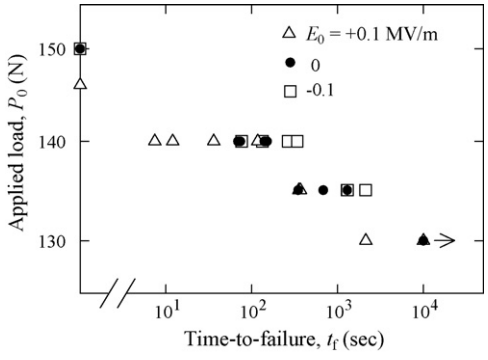

Fig. 4. Static fatigue curves of PCM-80 under $E_0 = +0.1, 0$, and -0.1 MV/m.

Table 2
Number of specimens used in the static fatigue tests

Applied electric field, E_0 (MV/m)	No. of tests	No. of samples failed on loading	No. of run out samples*
+0.1	12	4	1 (130)
0	8	0	1 (130)
− 0.1	8	1	0

* Data in parentheses represents the values of applied load.

similar to that of other non-piezoelectric brittle materials.[14,15] Times-to-failure of the PZT under $E_0 = +0.1$ MV/m and $E_0 = -0.1$ MV/m occur at each load level significantly lower and higher than that determined for $E_0 = 0$ V/m, respectively. This discrepancy can be attributed to the differences in stress distribution in the tests. Table 3 compares the experimentally measured average time-to-failure under $E_0 = +0.1, 0$, and -0.1 MV/m. Decrease (increase) of the time-to-failure under a positive (negative) electric field results from changes, under constant mechanical loading, in the shape and/or length of minute cracks. These changes take place in the presence of the electric fields which can react with newly formed surfaces of a growing crack. Thus the rate of crack growth under constant mechanical loading (static fatigue rate) may involve a change in the shape of the crack tip and a corresponding change in the electroelastic field concentrations.

The difference between the static fatigue fracture surface and catastrophic quasi-static (bend) fracture surface is illustrated in Fig. 5 for $E_0 = +0.1$ MV/m. The contact between the mating crack surfaces is seen to result in a "flattening" of the fracture surface asperities during static fatigue. Although the primary mechanism of fatigue fracture was intergranular separation, occasionally a small fraction of the grains observed on the fracture surface exhibited transgranular cleavage (Fig. 5(a)). Fig. 6 shows the similar micrographs for $E_0 = -0.1$ MV/m. The micrograph reveals a predominantly intergranular fracture path, as in Fig. 6(a). The PZT ceramics under a negative electric field have the greatest resistance for long time loads (see Table 3), and exhibit a larger degree of intergranular cracking compared to the PZT ceramics under a positive electric field.

The final crack lengths before failure measured with the microscope were about 0.9 mm. Results of static fatigue tests with different E_0 are shown in Fig. 7 as a plot of energy release rate against time-to-failure of PCM-80 for $a/W = 0.18$. Fatigue lives were observed to increase with the decrease in energy release rate. Time-to-failure, t_f (s), as a function of the energy

Table 3
Effect of applied electric field on time-to-failure of PCM-80 subjected to static load

Electric field, E_0 (MV/m)	Average time-to-failure t_f (s)	
	$P_0 = 135$ N	$P_0 = 140$ N
+0.1	361	43
0	776	108
−0.1	1573	203

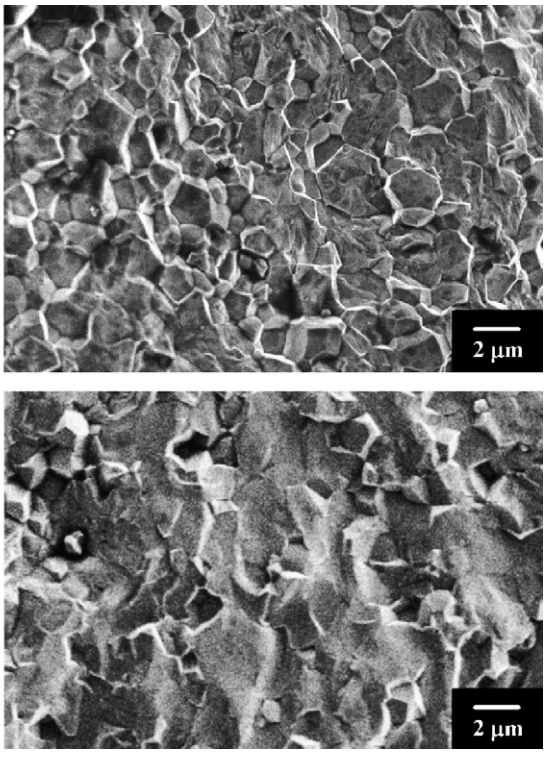

Fig. 5. Representative scanning electron micrographs morphologies obtained in PCM-80 under $E_0 = +0.1$ MV/m for (a) static fatigue fracture and (b) overload fracture.

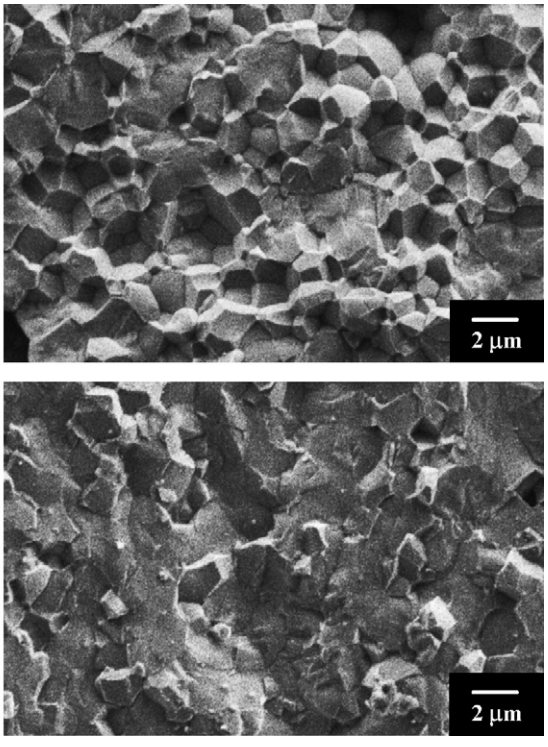

Fig. 6. Representative scanning electron micrographs morphologies obtained in PCM-80 under $E_0 = -0.1$ MV/m for (a) static fatigue fracture and (b) overload fracture.

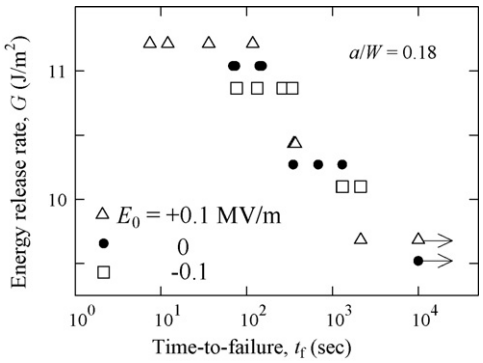

Fig. 7. Energy release rate vs. time-to-failure of PCM-80 under $E_0 = +0.1$, 0, and -0.1 MV/m.

release rate, G (J/m^2), can be expressed by

$$\begin{aligned} t_f &= 1.72 \times 10^{31} G^{-27.9} \quad (E_0 = -0.1\,\text{MV/m}) \\ t_f &= 2.43 \times 10^{30} G^{-27.2} \quad (E_0 = 0\,\text{MV/m}) \\ t_f &= 4.76 \times 10^{29} G^{-26.7} \quad (E_0 = +0.1\,\text{MV/m}) \end{aligned} \tag{24}$$

Although experimental data show scatter, at a G of 10 J/m^2, the time-to-failure is predicted to be 2165 s at $E_0 = -0.1$ V/m and 950 s at $E_0 = 0.1$ MV/m, for example. The experimental data suggest that there is an influence of electric field on the t_f versus G curve.

5. Conclusions

Static fatigue of cracked piezoelectric ceramics under electromechanical loading was studied using a three-point bending technique. Times-to-failure were obtained as a function of applied load, energy release rate, and electric field. Based on this experimental and numerical work, the following conclusions can be made.

1. The time-to-failure under a positive electric field was significantly shorter than under a negative electric field.
2. On the microscopic level, the mode of crack growth under a negative electric field was primarily intergranular. Traces of transgranular patterns were observed under a positive electric field.
3. Obtained static fatigue curves could be used to judge which piezoelectric ceramics would exhibit good resistance for long time load and which would not.

Acknowledgement

This work was partially supported by a Grant-in-Aid for Scientific Research (B) from the Ministry of Education, Culture, Sports, Science and Technology, Japan.

Appendix A

For piezoelectric ceramics which exhibit symmetry of a hexagonal crystal of class 6 mm with respect to principal x_1, x_2, and x_3 axes, the constitutive relations can be written in the

following form:

$$\begin{Bmatrix}\sigma_1\\ \sigma_2\\ \sigma_3\\ \sigma_4\\ \sigma_5\\ \sigma_6\end{Bmatrix} = \begin{bmatrix} c_{11} & c_{12} & c_{13} & 0 & 0 & 0\\ c_{12} & c_{11} & c_{13} & 0 & 0 & 0\\ c_{13} & c_{13} & c_{33} & 0 & 0 & 0\\ 0 & 0 & 0 & c_{44} & 0 & 0\\ 0 & 0 & 0 & 0 & c_{44} & 0\\ 0 & 0 & 0 & 0 & 0 & c_{66}\end{bmatrix} \begin{Bmatrix}\varepsilon_1\\ \varepsilon_2\\ \varepsilon_3\\ \varepsilon_4\\ \varepsilon_5\\ \varepsilon_6\end{Bmatrix} - \begin{bmatrix} 0 & 0 & e_{31}\\ 0 & 0 & e_{31}\\ 0 & 0 & e_{33}\\ 0 & e_{15} & 0\\ e_{15} & 0 & 0\\ 0 & 0 & 0\end{bmatrix} \begin{Bmatrix}E_1\\ E_2\\ E_3\end{Bmatrix} \tag{A.1}$$

$$\begin{Bmatrix}D_1\\ D_2\\ D_3\end{Bmatrix} = \begin{bmatrix} 0 & 0 & 0 & 0 & e_{15} & 0\\ 0 & 0 & 0 & e_{15} & 0 & 0\\ e_{31} & e_{31} & e_{33} & 0 & 0 & 0\end{bmatrix} \begin{Bmatrix}\varepsilon_1\\ \varepsilon_2\\ \varepsilon_3\\ \varepsilon_4\\ \varepsilon_5\\ \varepsilon_6\end{Bmatrix} + \begin{bmatrix} \in_{11} & 0 & 0\\ 0 & \in_{11} & 0\\ 0 & 0 & \in_{33}\end{bmatrix} \begin{Bmatrix}E_1\\ E_2\\ E_3\end{Bmatrix} \tag{A.2}$$

where

$$\sigma_1 = \sigma_{11}, \quad \sigma_2 = \sigma_{22}, \quad \sigma_3 = \sigma_{33}, \quad \sigma_4 = \sigma_{23} = \sigma_{32},$$
$$\sigma_5 = \sigma_{31} = \sigma_{13}, \quad \sigma_6 = \sigma_{12} = \sigma_{21} \tag{A.3}$$

$$\varepsilon_1 = \varepsilon_{11}, \quad \varepsilon_2 = \varepsilon_{22}, \quad \varepsilon_3 = \varepsilon_{33}, \quad \varepsilon_4 = 2\varepsilon_{23} = 2\varepsilon_{32},$$
$$\varepsilon_5 = 2\varepsilon_{31} = 2\varepsilon_{13}, \quad \varepsilon_6 = 2\varepsilon_{12} = 2\varepsilon_{21} \tag{A.4}$$

$$c_{11} = c_{1111} = c_{2222}, \quad c_{12} = c_{1122}, \quad c_{13} = c_{1133} = c_{2233},$$
$$c_{33} = c_{3333}, \quad c_{44} = c_{2323} = c_{3131},$$
$$c_{66} = c_{1212} = \frac{1}{2}(c_{11} - c_{12}) \tag{A.5}$$

$$e_{15} = e_{131} = e_{223}, \quad e_{31} = e_{311} = e_{322}, \quad e_{33} = e_{333} \tag{A.6}$$

References

1. Park, S. and Sun, C.-T., Fracture criteria for piezoelectric ceramics. *J. Am. Ceram. Soc.*, 1995, **78**, 1475–1480.
2. Fu, R. and Zhang, T.-Y., Effects of an electric field on the facture toughness of poled lead zirconate titanate ceramics. *J. Am. Ceram. Soc.*, 2000, **83**, 1215–1218.
3. Shindo, Y., Murakami, H., Horiguchi, K. and Narita, F., Evaluation of electric fracture properties of piezoelectric ceramics using the finite element and single-edge precracked-beam methods. *J. Am. Ceram. Soc.*, 2002, **85**, 1243–1248.
4. Soh, A. K., Fang, D.-N. and Lee, K. L., On the effects of an electric field on the fracture toughness of poled piezoelectric ceramics. *Mater. Sci. Eng. A*, 2003, **360**, 306–314.
5. Jelitto, H., Kebler, H., Schneider, G. A. and Balke, H., Fracture behavior of poled piezoelectric PZT under mechanical and electrical loads. *J. Euro. Ceram. Soc.*, 2005, **25**, 749–757.
6. Shindo, Y., Narita, F., Horiguchi, K., Magara, Y. and Yoshida, M., Electric fracture and polarization switching properties of piezoelectric ceramic PZT studied by the modified small punch test. *Acta Mater.*, 2003, **51**, 4773–4782.
7. Shindo, Y., Narita, F. and Mikami, M., Double torsion testing and finite element analysis for determining the electric fracture properties of piezoelectric ceramics. *J Appl Phys*, 2005, **97**, 114109.
8. Cao, H. C. and Evans, A. G., Electric-field-induced fatigue crack growth in piezoelectrics. *J. Am. Ceram Soc*, 1994, **77**, 1783–1786.
9. Weitzing, H., Schneider, G. A., Steffens, J., Hammer, M. and Hoffmann, M. J., Cyclic fatigue due to electric loading in ferroelectric ceramics. *J. Euro. Ceram. Soc.*, 1999, **19**, 1333–1337.
10. Lee, K. L., Soh, A. K. and He, P. F., Fatigue failure of ferroelectric ceramics subjected to cyclic inclined electric loading. *Scripta Mater.*, 2003, **49**, 849–854.
11. Fang, D., Liu, B. and Sun, C. T., Fatigue crack growth in ferroelectric ceramics driven by alternating electric fields. *J. Am. Ceram. Soc.*, 2004, **87**, 840–846.
12. Salz, C. R. J., Hoffman, M., Westram, I. and Rodel, J., Cyclic fatigue crack growth in PZT under mechanical loading. *J. Am. Ceram. Soc.*, 2005, **88**, 1331–1333.
13. Su, Y. J., Wang, Y., Chu, W. Y., Gao, K. W. and Qiao, L. J., Combined effect of electric and mechanical loading on fracture of the PZT-5 ferroelectric ceramics. *Acta Mater.*, 2004, **52**, 3753–3759.
14. Krohn, D. A. and Hasselman, D. P. H., Static and cyclic fatigue behavior of a polycrystalline alumina. *J. Am. Ceram. Soc.*, 1972, **55**, 208–210.
15. Ritter, J. E. and Humenik Jr., J. N., Static and dynamic fatigue of polycrystalline alumina. *J. Mater. Sci.*, 1979, **14**, 626–632.